DOI: 10.1002/ejic.201100329

Effect of Electrode Dimensionality and Morphology on the Performance of Cu_2Sb Thin Film Electrodes for Lithium-Ion Batteries

Lynn Trahey,[a,b] Harold H. Kung,[b] Michael M. Thackeray,[a] and John T. Vaughey*[a]

Dedicated to Professor John D. Corbett on the occasion of his 85th birthday

Keywords: Electrochemistry / Thin films / Copper / Antimony / Intermetallic phases

Although graphitic carbons have been commercially used in lithium-ion batteries for many years, their low crystallographic density limits their use in applications where space is at a premium. Among the alternative anode materials being considered for these applications are Zintl phases and intermetallic insertion anodes. Historically, main-group-metal-based anode materials have had problems with respect to volume expansion experienced on lithiation and its effect on cycle life. In this paper, we report the role of morphology and electrode dimensionality in extending the cycle life of the intermetallic insertion anode Cu_2Sb. We have found that controlling the surface area of the active material and building internal volume into the electrode structure significantly decreases the capacity fade on cycling. The decrease in fade rate may be due to the active material gradient identified within the structure produced by the electrodeposition process. This enhancement in cycling can be attributed to keeping the displaced copper closer to the active particles and to reducing the diffusion distances within the electrode.

Introduction

Lithium-ion batteries are a complex electrochemical system where numerous variables must be controlled and optimized to achieve a functioning battery. Not only must individual electrode materials be developed, but their incorporation into an electrode and full cell also represent additional hurdles to be overcome in verifying the utility of any new materials. As new applications for lithium-ion batteries are proposed, advances in battery materials are needed to meet the new end-user requirements. Many of the newer applications require anode materials that possess a high volumetric capacity (mA h/cc) in addition to a gravimetric capacity (mA h/g) in excess of that of commercialized graphitic carbons.[1–3] To date, several types of materials that meet these requirements have been identified; they include a variety of NiAs-related intermetallic materials and lithium Zintl phases.[4–8] The most basic materials under consideration are the lithium-containing Zintl phases. These high-capacity materials, for example Li_xSi, can store up to an order of magnitude more lithium per unit mass than conventional graphitic carbon; however, whereas graphitic carbons expand by 15% on full lithiation (to LiC_6), the most studied lithium Zintl phases, $Li_{17}Sn_4$ and $Li_{15}Si_4$, typically expand by as much as 450%.[9–12] These large volume changes on lithiation (compared to the volume of the element) introduce a variety of problems when the materials are incorporated into a sealed electrochemical cell. Solutions to these issues have included development of new polymeric binders that can maintain the necessary connectivity between the active material and the electrode surface and bonding the active material directly to the underlying anode current collector.[13–17]

A second approach is to use intermetallic insertion electrodes, where the lithium cations are inserted into vacancies within an intermetallic compound to form, in the simplest case, a ternary compound.[18–20] Typical materials that have been studied include compounds in the MnSb–LiMnSb and the Cu_2Sb–Li_2CuSb systems.[21–22] As can be noted, the metal ratio of the initial material is, although not in all cases, slightly different from that of the charged material. In these cases, the reactions are still reversible, but within an electrode structure, the displacement of a metal must be taken into account so as to ensure its availability for the back reaction. This reformation step has the following benefit: when the displaced metal diffuses back into the delithiating main group metal to reform the intermetallic compound, it has the effect of suppressing main group metal agglomeration on cycling, a common failure mechanism for Zintl phase anodes.[23,24] The gravimetric capacities of many of these materials are similar to that of graphitic carbon but their volumetric capacities are as much as three times greater. In this study, the role of electrode dimensionality

[a] Chemical Sciences and Engineering Division, Argonne National Laboratory,
Argonne, IL 60439, USA
[b] Department of Chemical and Biological Engineering, Northwestern University,
2145 Sheridan Rd, Evanston, IL 60208, USA

and morphology of a series of Cu_2Sb thin film anode structures were investigated. Materials were synthesized by using electrodeposition of copper and antimony onto a porous copper lattice or a flat copper foil and annealing to create the working electrode structure. This type of study will give insights into the role that electrode dimensionality and internal porosity play in keeping the displaced copper active throughout the battery cycling process.

Results and Discussion

In this study we have examined the role of electrode dimensionality and morphology on the reversibility of a Cu_2Sb thin film electrode material. This intermetallic compound has been reported to have a reversible capacity similar to that of graphite with an approximate volume expansion of 42% between the fully discharged starting material and the fully lithiated charged electrode material. The volumetric expansion of graphite in going from C_6 to LiC_6 has been reported to be 10–15%. The complete reaction, including the formation of the ternary compound Li_2CuSb around 0.5 V, is shown below.

$$Cu_2Sb + 2\ Li \rightleftharpoons Li_2CuSb + Cu$$

$$Li_2CuSb + x\ Li \rightleftharpoons (Li_{3-x}Cu_x)Sb + 1-x\ Cu$$

Although the material has been demonstrated to have a reversible capacity of > 300 mA h/g (or > 2100 mA h/cm^3), its long-term stability when cycling over the complete voltage range (0–1.5 V) has been hindered by the requirement that the copper extruded on lithiation (charge) still be available to reform the starting compound on delithiation (discharge). Because these displacement reactions can be dependent upon the morphology of the sample, we varied our electrodeposition method to form Cu_2Sb films with two different morphologies. Starting from an acidified aqueous solution containing copper and antimony in the correct stoichiometric ratio, we employed two different galvanostatic square-wave pulse sequences that yielded either a cauliflower-type film (GSW-1) or a flat film (GSW-2). Figure 1 shows a typical CV curve for this solution. The higher-surface-area GSW-1 film is anticipated to have faster kinetics as a larger percentage of the active material is in contact with the electrolyte; however, it also should lose capacity faster as the active material becomes electronically isolated and is physically separated from the current collector as a result of the repeated volume changes on cycling. In contrast, the flatter film produced by using the GSW-2 pulse sequence should have better stability, as the active material has a less tenuous connection to the current collector, but the lithium diffusion distance should be longer on average. Figure 2 highlights the two different morphologies produced with the two different deposition routines. Experimentally, these two types of films were deposited in equal amounts on a flat copper foil substrate. The electrochemical cycling performance of these two films is shown in Figure 3. Because solid electrolyte interphase (SEI) formation obscures the true reversible electrochemical activity of anode materials in the first cycle and the weights of the electrodeposited and annealed active materials are not known with high enough recision, the data are normalized to the second cycle capacities. It is evident from the data that the rougher, higher-surface-area film, has a more dramatic fade rate. This is in agreement with the fact that repeated lithium insertion and removal causes loss of active material – either physically or through electronic isolation. SEM analysis of the cycled flat-morphology film electrode is shown in Figure 4, and it can be seen that even the more stable electrode experienced significant cracking and fracturing.

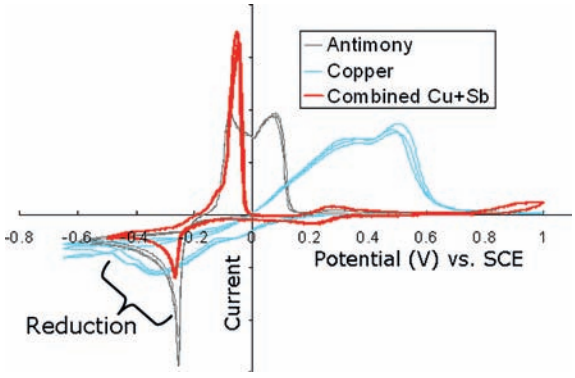

Figure 1. Cyclic voltammetry (CV) curve for the solution used to electrodeposit copper antimonide in comparison to the individual elements involved.

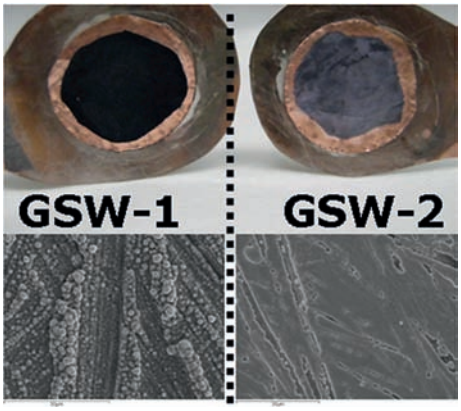

Figure 2. Images of the two types of morphologies generated by the two different pulse sequences used for the electrodeposition. Scale bars in bottom SEM images are both 30 μm.

A prominent fade mechanism for these materials on repeated cycling is the inability of the copper displaced on charge to remain close enough to the reaction zone to reform the starting material on discharge. This problem can be addressed by going to a three-dimensional electrode structure, which should keep the displaced copper in the interior of the electrode, inhibiting its ability to move through the SEI layer into the electrolyte. To investigate this hypothesis, the same two types of films were deposited into a three-dimensional porous copper substrate made by a method previously published.[25] Figure 5 shows SEM photos of the two types of films on the three-dimensional electrode substrate. The electrochemical cycling of these three-

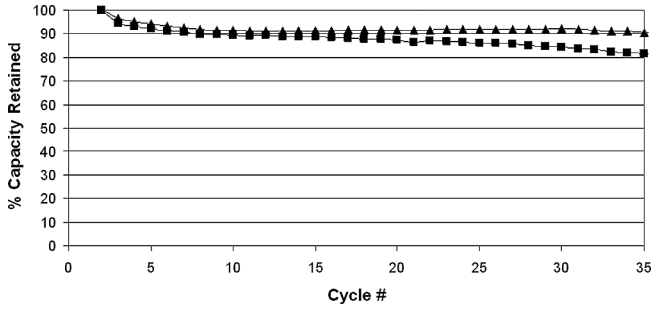

Figure 3. Effect of morphology on the cycling fade rate of two thin film two-dimensional electrodes: (▲) data from a flat-morphology film, (■) data from a rough-morphology film.

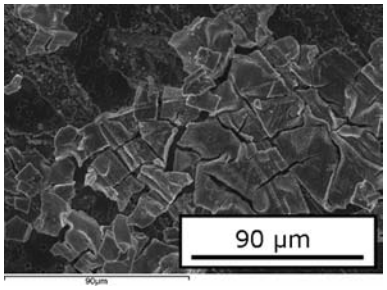

Figure 4. SEM image of the cycled flat-morphology film electrode with evidence of significant cracking and fracturing on long-term cycling.

dimensional electrodes with a rough or flat surface film is shown in Figure 6. As was seen with the two-dimensional substrate, the flat thin film morphology again had a lower fade rate on the three-dimensional substrate than the rougher film.

When comparing all of the samples studied, the best samples are the flatter thin film morphology combined with the three-dimensional substrate. The worst performing sample was the rough thin film morphology on the three-dimensional substrate, which lost nearly thirty percent of its capacity by the tenth cycle. Considering the electrochemical and electron microscopic evidence form both studies, it is probable that the space restrictions the three-dimensional substrate places on rough films during deposition may result in overall weaker connections to the current collector. This weakness would result in more active material loss as a result of the volume expansion and contraction on cycling in comparison to electrode structures with less surface area.

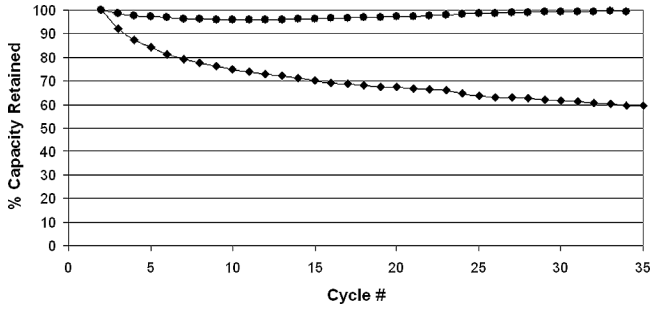

Figure 6. Effect of morphology on the cycling fade rate of two thin film three-dimensional electrodes: (●) data from a flat-morphology film, (♦) data from a rough-morphology film.

In order to further investigate the differences between the two electrodes, we performed an in-depth study of the three-dimensional electrode by using the four-point nanoprobe at the Center for Nanoscale Materials at Argonne National Laboratory. In this instrument, the conductivity of a sample can be determined as a function of depth within the electrode. The overall morphology of the sample and an SEM image of the STM tips on the sample are shown in Figure 7. The data indicates that, as a function of cycle number, the lower regions of the electrode show only small changes in resistance when compared with the higher regions of the electrode. Table 1 shows the differences in resistance as a function of cycle number and depth within the electrode. This dramatic change in resistivity near the electrolyte–electrode surface on cycling can be ascribed to the formation and electronic isolation of semiconducting $(Li_{3-x}Cu_x)Sb$ (and small amounts of $Li_{17-x}Cu_xSn_4$) phases combined with encapsulation of displaced copper by the SEI layer. Figure 8 highlights the post-cycling morphology of the three-dimensional electrodes near the interfaces with the electrolyte and with the current collector. Even after cycling, the lower echelons of the electrode contain larger particles and display rougher active particle morphologies than the top section, where the active materials have been pulverized and coated by a thicker SEI layer. The dramatic differences indicate that the surface of the porous electrode has been more deeply cycled than the active material in the depths of the electrode pores. This inhomogeneity formed on cycling may be a result of the volume expansion inside the porous electrode closing off inner pores and forcing out the liquid electrolyte. Under these circumstances, the active

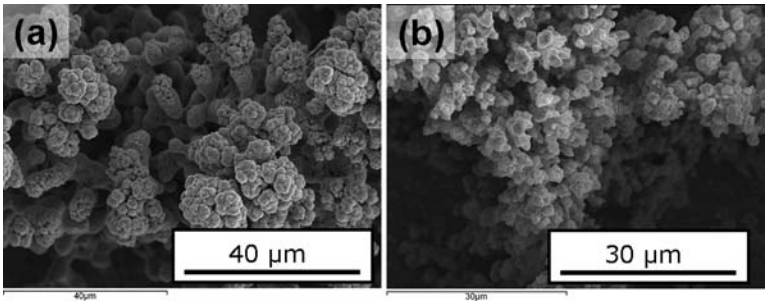

Figure 5. SEM micrographs of the two types of films deposited on the three-dimensional electrode substrate using (a) galvanic square wave 1, and (b) galvanic square wave 2.

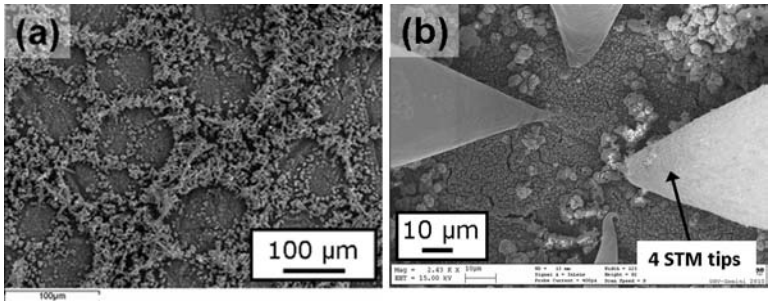

Figure 7. SEM micrographs of the (a) overall morphology of the three-dimensional electrode used for 4-pt nanoprobe studies, and (b) low-altitude region with STM tips on the sample.

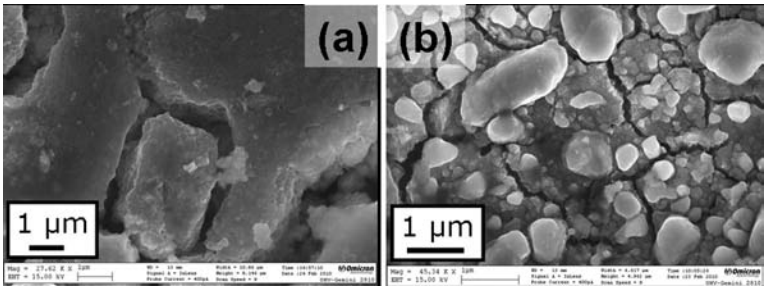

Figure 8. SEM micrographs of the electrode-active particles (a) on the top region of the electrode and (b) bottom of the electrode, both after cycling.

material in the deepest parts of the electrode would contribute less capacity than the surface active materials while undergoing less dramatic volume shifts. This graduated lithiation may also contribute to the stability of the electrode by mediating the volume expansion stresses induced at the interface between the copper foil and the porous copper substrate. A similar mechanism for structured anodes has been proposed for nanowire arrays.[11,26]

Table 1. Resistivity of a three-dimensional Cu_2Sb electrode as a function of cycle number and electrode depth.

Cycle number	Top of electrode (Ω)	Bottom of electrode (Ω)
20	10^{-3}	10^{-4}
30	10^{-2}	10^{-5}
45	10^{0}	10^{-5}
52	too high	10^{-4}

Conclusions

We have investigated the advantages of using a three-dimensional current collector that provides space within the electrode for the displaced copper produced on charging Cu_2Sb. We found that for either a two or a three-dimensional anode electrode structure, more stable performance was obtained when the Cu_2Sb active material thin film was smooth, with less surface area in contact with the electrolyte. When combined with internal porosity, the flat film in combination with a three-dimensional electrode structure displayed the most stable (least amount of capacity fade) cycling. This enhanced stability was found to be partly due to the extension of the active surface area into the electrode pore structure, which kept the displaced copper formed on charge closer to the reaction site. Further work will examine various methods to get a more even coating throughout the three-dimensional electrode and enhanced electrode utilization.

Experimental Section

The reduction potentials of divalent copper and trivalent antimony were first determined at room temperature by cyclic voltammetry (CV) in a solution of $CuCl_2{\cdot}2H_2O$ (0.01 M) and $SbCl_3$ (0.01 M) with HCl (10 vol.-%). The CV experiments were performed by using an electrochemical cell with a Pt disk working electrode, a Pt gauze counterelectrode, and a saturated calomel reference electrode (SCE); a sweep rate of 50 mV/s was employed. The solutions for the deposition of Cu_2Sb films on copper substrates consisted of $CuCl_2{\cdot}2H_2O$ (0.04 M), $SbCl_3$ (0.02 M), and HCl (12 vol.-%). The films were deposited by using two different galvanostatic square waves designed to deposit identical total masses. Program (1) step 1: –10 mA, 30 s; step 2: 0 mA, 10 s; repeated 20 times. Program (2) step 1: –10 mA, 1 s; step 2: –1 mA, 10 s; repeated 300 times. All depositions were carried out with a PAR 273A potentiostat/galvanostat and were made, while stirring the solutions, on stainless steel, copper foil, and sintered porous copper substrates at room temperature. The coated substrates were subsequently annealed at 200 °C for 4 h under an argon atmosphere.

Porous copper current collectors were fabricated on copper foil substrates by electrodeposition following a procedure previously published.[25] The deposition solution consisted of $CuSO_4{\cdot}5H_2O$ (0.2 M) and H_2SO_4 (1.5 M) for the Cu_2Sb experiments. Depositions were performed for 70 s at room temperature without stirring. The counterelectrode was copper gauze, and the applied current was –1.33 A. In order to identify and define the limits of the upper

and lower regions of the porous copper electrode for the four-point nanoprobe experiments, HCl (10 mM) was added to the bath and depositions were stopped after 20 s. The resulting porous copper substrates were sintered at 500 °C for 45 h under an argon atmosphere. Copper and antimony were deposited onto porous copper current collectors by using the solutions previously described and Program 2 (described above) for 150 cycles. These electrodes were annealed at 150 °C for 24 h in an argon environment. XRD of the annealed electrodes showed primarily the phase Cu_2Sb. For the final films used in the four-point nanoprobe study, a few weight percent tin was added to the film during deposition to control the diffusion of copper at low voltage and high lithiation.[25,27] First, Cu and Sb were deposited by using the solution and Program 2 for 150 cycles. Subsequently, Sn was deposited from a bath of $SnSO_4$ (0.02 M), tartaric acid (0.2 M), and sodium sulfate (1 M) by using another galvanic square wave procedure (step 1: –10 mA, 1 s; step 2: –1 mA, 5 s; repeated 120 times). After annealing at 150 °C for 24 h in an argon environment, XRD analysis of the annealed electrodes showed primarily Cu_2Sb and the tin segregated into SbSn, Cu_6Sn_5, and elemental tin.

All electrodes were assembled and evaluated in 2032 coin cells containing a metallic lithium counterelectrode, a Celgard separator, and $LiPF_6$ (1.2 M) in ethylene carbonate/ethyl methyl carbonate (30:70 wt.-%) electrolyte. Coin cells were cycled galvanostatically at 0.08 mA from 0 to 1.5 V at room temperature. If electrodes were analyzed after cycling, they were extracted from the coin cell in a glove box and rinsed with dimethyl carbonate. Electrodes were analyzed by scanning electron microscopy (SEM, JEOL 6400), energy-dispersive X-ray spectrometry (EDS, Oxford INCA), and X-ray diffraction (XRD, Siemens D5000). Four-point nanoprobe experiments were conducted by using the Omicron UHV Nanoprobe at the Center for Nanoscale Materials at Argonne National Laboratory. Keithley 6430 and 2182 instruments were used as the current source and voltmeter, respectively. Typical currents for four-point resistivity measurements were 1–8 mA.

Acknowledgments

The authors would like to acknowledge support for the Cu_2Sb study from the Batteries for Advanced Transportation Technologies (BATT) Program of the U.S. Department of Energy under Contract No. DEAC02-06CH11357, the Northwestern University Center for Energy Efficient Transportation, and the Northwestern University Institute for Sustainability and Energy. Four-point nanoprobe work was supported by the Center for Electrical Energy Storage: Tailored Interfaces, an Energy Frontier Research Center funded by the U.S. Department of Energy, Office of Science, Office of Basic Energy Sciences. Use of the four-point nanoprobe at the Center for Nanoscale Materials (CNM) at Argonne National Laboratory is also acknowledged.

[1] A. S. Arico, P. Bruce, B. Scrosati, J. M. Tarascon, W. Van Schalkwijk, *Nat. Mater.* **2005**, *4*, 366.
[2] S. G. Chalk, J. E. Miller, *J. Power Sources* **2006**, *159*, 73.
[3] R. Gilbert, *J. Urban Technol.* **2010**, *17*, 53.
[4] K. Gallagher, P. Nelson, D. Dees, *J. Power Sources* **2011**, *196*, 2289.
[5] H. Kim, J. Cho, *Nano Lett.* **2008**, *8*, 3688.
[6] R. Krishnan, T. M. Lu, N. Koratkar, *Nano Lett.* **2011**, *11*, 377.
[7] P. Limthongkul, Y. Jang, N. Dudney, Y. M. Chiang, *Acta Materialia* **2003**, *51*, 1103.
[8] M. Park, K. Kim, J. Kim, J. Cho, *Adv. Mater.* **2010**, *22*, 415.
[9] A. Kamali, R. Fray, *Rev. Adv. Mater. Sci.* **2011**, *27*, 14.
[10] L. Beaulieu, D. Larcher, R. Dunlap, J. Dahn, *J. Electrochem. Soc.* **2000**, *147*, 3206.
[11] C. Chan, H. Peng, G. Liu, K. MacIwrath, X. Zhang, R. Huggins, Y. Cui, *Nature Nanotechnol.* **2008**, *3*, 31.
[12] M. Datta, P. Kumta, *J. Power Sources* **2006**, *158*, 557.
[13] Y. Gao, M. Zhou, *J. Appl. Phys.* **2011**, *109*, 14310.
[14] M. Song, Y. Kim, J. Cho, B. Cho, B. Popov, H. Rhee, *J. Power Sources* **2004**, *125*, 10.
[15] D. Chang, S. Lee, S. Kim, H. Kim, *J. Power Sources* **2002**, *112*, 452.
[16] K. Xu, C. Angell, *J. Electrochem. Soc.* **1998**, *145*, L70.
[17] H. Bryngelsson, M. Stjerndahl, T. Gustafsson, K. Edstrom, *J. Power Sources* **2007**, *174*, 970.
[18] H. Bryngelsson, M. Stjerndahl, T. Gustafsson, J. Vaughey, M. Thackeray, K. Edstrom, *Electrochim. Acta* **2007**, *52*, 4947.
[19] J. Vaughey, K. Kepler, R. Benedek, M. Thackeray, *Electrochem. Commun.* **1999**, *1*, 517.
[20] S. Song, P. Reade, E. Cairns, J. Vaughey, M. Thackeray, K. Striebel, *J. Electrochem. Soc.* **2004**, *151*, 1012.
[21] L. Fransson, J. Vaughey, K. Edstrom, M. Thackeray, *J. Electrochem. Soc.* **2003**, *150*, 86.
[22] E. Perre, P. Taberna, D. Mazouzi, P. Poizot, T. Gustafsson, K. Edstrom, P. Simon, *J. Mater. Res.* **2010**, *25*, 1485.
[23] Y. Wang, J. Lee, B. Chen, *J. Electrochem. Soc.* **2004**, *151*, 563.
[24] J. Yang, M. Wachtler, M. Winter, J. Besenhard, *Electrochem. Solid-State Lett.* **1999**, *2*, 161.
[25] L. Trahey, J. Vaughey, H. Kung, M. Thackeray, *J. Electrochem. Soc.* **2009**, *156*, 385.
[26] N. Wang, Y. Cai, R. Q. Zhang, *Mat. Sci. Eng. R Rep.* **2008**, *60*, 1.
[27] A. N. Jansen, J. Clevenger, A. Baebler, J. T. Vaughey, *J. Alloys Compd.* **2011**, *509*, 4457.

Received: March 29, 2011
Published Online: August 9, 2011

